On High Temperature Materials: An Overview of Deformation and Fracture Maps of a Super Alloy Stainless Steel by Analytical Modeling

A. Kanni Raj

Professor - School of Basic Sciences
Vel Tech Rangarajan
Dr. Sagunthala R&D Institute of Science & Technology
Chennai, (T.N.) [INDIA]
Email: akanniraj@yahoo.com

ABSTRACT

This rapid publication article is on the creep behavior of AISI 310S stainless steel taken from SAIL's Salem stainless steel plant, and computational technique was used to model deformation and fracture at the temperatures of 973-1073K and loads of 40-150MPa. Computer program coded in C++ was used to plot deformation and fracture maps. It is inferred that in all test temperatures, power-law creep due to dislocation climb is operating mechanism of creep deformation. Above temperatures and loads supports formation of grain boundary voids and cracks leading to inter-granular creep fracture. Experiments proved these predictions.

Keywords:— Stainless Steel, Creep, Deformation Map, Climb, Fracture Map, Wedge Crack.

I. INTRODUCTION

Materials operating at high temperature are subjected to creep, hot corrosion, erosion, and phase change which severely affect the temperature capability and load bearing capacity of materials [1]. AISI 310S stainless steel contains higher chromium and nickel content than common iron-based alloys. It is a standardized high-temperature steel for use at temperatures of up to 1323 K in dry air. It has a unique combination of high strength and superior oxidation resistance for application up to 1323 K [2]. It is also very ductile and has good welding capability enabling its widespread usage in many applications. It finds wide application in all high-temperature environments where scaling and corrosion resistance, as well as high temperature strength and good creep resistance, are required. Because of its super-alloy properties, this alloy is a likely candidate material for high-temperature applications [1, 2]. It is a nonmagnetic alloy that cannot be hardened by heat treatment. It has forming capabilities similar to that of AISI 304 stainless steel. It can be easily formed into most shapes. Extended capabilities of this stainless steel, beyond that of conventional stainless steels, make it potentially viable to replace nickel-based super alloys. A quantum of information connected with processing, tensile properties, oxidation, hot corrosion, deformation and fracture behavior of this alloy is available in the literature. The current research project focuses on the computational identification of deformation and fracture mechanism of creep of sheet samples taken from production run of Indian government stainless steel giant SAIL [2]. Complete experimental analyses of creep and hot corrosion are presented

elsewhere and a comparison as a proof for theoretical outputs is given in this article here and there [2].

II. THEORETICAL PROCEDURES

Creep Deformation Equations

Polycrystalline material deform by several different mechanisms when stressed. A plot of normalized tensile stress and homologous temperature is called deformation map. The maps display the domains of stress and temperature in which a particular mechanism of plastic flo is dominant. A point on a map then identifies the dominant mechanism and indicates the resulting minimum cree rate [1-4]. The present investigation has been undertaken to generate a deformation mechanism map for AISI 310 stainless stee sheets and to study the deformation mechanism involved in the short-term cree of AISI 310S austenitic stainless steel at an applied temperature range of 973-1073K for an applied stres ranging of 40-150MPa. Besides constructing the deformation mechanism map and analyzing the mechanism involved in the creep deformation using the map, the mechanism involved in the creep deformation of AISI 310S stainless steel sheets is also analyzed based on stress exponen (n) and creep activation energ (Qc).

During the cree deformation of a polycrystalline material, the steady state cree rate ($\dot{\varepsilon}_s$) is, generally described by an empirical power-law function of applied stres (σ) as follows:

$$\dot{\varepsilon}_s = A'\sigma^n e^{\frac{-Q_c}{RT}} \qquad \ldots\ldots\ldots\ldots\ldots(1)$$

Where A' is a constant, R is the universal gas constant and T is absolute temperature. Basic theory of the above empirical equation has been illustrated by various researchers [2]. At temperatures above the half of melting point and relatively high stresses, dislocations move through the grains of a polycrystalline material and aggregate to form cells. This first mechanism constitutes power-law cree or recover controlled creep which is represented by the following power-law equation:

$$\dot{\varepsilon}_s = \left(\frac{AD_{v_0}Gb}{kT}\right)\left(\frac{\sigma}{G}\right)^n e^{\frac{-Q_v}{RT}} \qquad \ldots\ldots\ldots\ldots(2)$$

Where A is a constant, D_{v0} is the lattice diffusio coefficient, G is shear modulus, b is the Burgers vector of the dislocation, k is the Boltzmann's constant and Qv is the activation energ for lattice diffusion. The second mechanism is the diffusio cree which becomes the controlling mechanism at high temperature and relatively low stresses. Nabbaro and Herring proposed that the creep process was controlled by stress-directed atomic diffusion of vacancie from grain boundaries and atoms in opposite direction. They arrived at the following equation:

$$\dot{\varepsilon}_s = \left(\frac{B\sigma D_{v_0}b^3}{kTd^2}\right)e^{\frac{-Q_v}{RT}} \qquad \ldots\ldots\ldots\ldots(3)$$

Where B is a constant and d is the grain size in the original theory, the diffusion was considered to occur only through the lattice. However, material can also diffuse along grain boundaries. This contribution to diffusion creep was first recognized by Coble. He presumed that at lower temperatures grain boundary diffusion predominates and derived the following equation:

$$\dot{\varepsilon}_s = \left(\frac{C\sigma D_{g_0}b^4}{kTd^3}\right)e^{\frac{-Q_g}{RT}} \qquad \ldots\ldots\ldots\ldots(4)$$

Where C is a constant, D_{g0} is the grain boundary diffusio coefficient and Q_g is the

activation energ for grain boundary diffusion.

The third mechanism occurs at very high (higher than power-law) stress level in which the metal deform by thermally activated dislocation glid. Creep formation resulting from a dislocation glide mechanism occurs at stress levels which are high relative to those normally considered in creep deformation. Equation corresponding to dislocation glide is given by:

$$\dot{\varepsilon}_S = Ee^{\frac{-\left(\frac{Gb}{l} - \sigma\right)ba}{kT}} \qquad \text{..................(5)}$$

Where E is a constant, 'a' is activation area and 'l' is the obstacle spacing. The last mechanism is the defect-less flow which occurs for the stress levels above the theoretical shear strengt of polycrystalline materials. As stated earlier, the various regions of the map indicate the dominant deformation mechanism for that stress-temperature combination. The boundaries of these regions are obtained by solving the above constitutive equations for stress as a function of temperature. The upper bound on the diagram is the stress to produce sli in a perfect (dislocation free) lattice i.e., theoretical shear strengt of the alloy. The theoretical shear strength is given by $\sigma = G/2\pi$. So the line corresponding to theoretical strengt is $\sigma/G = 1/2\pi$. Line corresponding to dislocation glide (in pure austenitic iron) is drawn at $\sigma/G = 5 \times 10^{-3}$. Another least possible mechanism to be considered is twinning. For FCC metals a twinning field appears at low temperatures; it typically exist only below about 20K. So it need not be considered while constructing the map.

Fracture Mechanism Equations

The cree fracture map was used for analyzing the mechanism of creep fracture in AISI 310 austenitic stainless stee sheets having an average grain size of 55 μm. The creep fracture mode predicted by the creep fracture map is usually verified by optical microscop. Inter-granular wedge crack (triple point crackin) was found to be the operating mechanism of creep fracture for AISI 310S stainless steel sheets. Polycrystalline material undergo fracture by several different mechanisms when subjected to an applied stres. The precise mode of fracture depends critically on testing conditions, such as stress and temperature, and on material parameters such as grain size and concentration of precipitates. A plot of normalized stress against homologous temperature showing different domains, within which a particular mechanism was dominant, is called fracture map [1, 2, 5]. A point on the map then identifies the dominant fracture mechanism and indicates the resulting time to fracture. The applications and limitations of the map are available elsewhere. The main objectives of the present investigation are as follows: (a) to generate a cree fracture map for AISI 310 austenitic stainless stee sheets having an average grain size of 55 μm in logarithmic normalized stres-reciprocal homologou temperature space, (b) to analyze the mechanism of cree fracture by conducting short-term creep-ruptur experiments on AISI 310 austenitic stainless stee under constant load (stress (σ) range 40-150MPa) at three different temperatures, viz., 973K, 1023K and 1073K, and (c) to compare the mechanism of cree fracture predicted by the creep fracture map and the experimental observations for AISI 310 austenitic stainless stee sheets. Various mechanisms of cree fracture and detailed derivations of equations for each mechanism are available in literature and in internet nowadays. Only a brief account of all constitutiv equations is given here. Time to rupture (tr) for trans-granular fractur is given by:

$$t_r = \left[\varepsilon_n + \left(\frac{1}{1.8}\right) \left(\frac{n}{n-1}\right) \ln\left(\frac{0.7}{f_v^{1/2}} - 1\right) \right] \dot{\varepsilon}_s^{-1} \qquad \text{.......(6)}$$

Where εn is the nucleation strain, n is the stress exponen, fv is the volume fraction of intra-granular inclusions and εs is the steady state cree rate. Time to rupture for triple point crackin is given by:

$$t_r = \frac{2\gamma}{Gd\xi} \left(\frac{\sigma}{G}\right)^{-1} \dot{\varepsilon}_s^{-1} \qquad \text{.........(7)}$$

Where 'γ' is effective surface energy for fractur, G is the shear modulus, d is the grain size, ξ is the contribution of grain boundary sliding to the total strain and σ is the applied stres. Time to rupture for cavitation by diffusio growth is given by:

$$t_r = \frac{6 \times 10^{-2} l^2}{\delta D_g b^2} \left(\frac{kT}{Gb}\right) \left(\frac{\sigma}{G}\right)^{-1} \qquad \text{.........(8)}$$

Where l is the average cavity spacing in the boundary, δ is the width of the grain boundary, Dg is the grain boundary diffusio coefficient, b is the Burgers vector, k is the Boltzmann's constant and T is the absolute temperature. Time to rupture for cavitation by power-law growth is given by:

$$t_r = \left[\frac{1 - 0.78\left(\frac{p_o}{l_o}\right)}{1.48} \right] \dot{\varepsilon}_s^{-1} \qquad \text{..............(9)}$$

Where p_o and l_0 are the average particle diameter and spacing along boundary respectively. Steady state cree rate for low temperature (LT) regime is given by "Equation 2". Steady state cree rate for high temperature (HT) regime is given by:

$$\dot{\varepsilon}_s = 50 A D_{g0} \left(\frac{Gb}{kT}\right) \left(\frac{\sigma}{G}\right)^{n+2} e^{\frac{-Q_g}{RT}} \qquad \text{.......(10)}$$

Where D_{g0} is grain boundary diffusio coefficient. The various domains and boundaries of cree fracture map for AISI 310 austenitic stainless stee sheets were obtained by solving these constitutiv equations for the time to rupture and for the steady state cree rate using C++ programming language. The inherent assumption in constructing the map is that the various fracture mechanisms operate independently.

III. RESULTS AND DISCUSSIONS

Deformation Mechanism Map

Though not required, for the sake of clarity, alloy chemistry and metallographic data are reported. The chemical composition was obtained accurately using vacuum evaporation spectrometer of the alloys considered in the analysis ("Table "). Usual optical metallographic procedure was used to get microstructure. The two-dimensional grain size was measured using Hayn intercep method. The microstructure mainly contains grain with a grain size of 55μm. The microstructure consists of two phases, namely, gamma and carbide phases. Twins are also seen. It is very hard to see distinctly anything at carbides at low magnifications. But optical micrographs clearly reveal the presence of the carbides inside grains ("Figure 1"). The main focus of the present investigation is the cree deformation mechanism of AISI 310 stainless stee sheet. Properties and constants used in the calculation of the boundaries in deformation mechanism map are taken from literature and internet ("Table 2"). A software using C++ programming language was developed to draw deformation mechanism map for AISI 310 stainless stee sheets (fully anneale condition with an average grain size of 55μm) by solving above constitutiv equations for various deformation mechanisms and to determine the various domains and

boundaries among them. From the deformation mechanism map ("Figure 2"), it is seen that the creep followed recovery controlled mechanism (power-law mechanism). Creep tests were conducted to check for this mechanism (in terms of experimental n and Qc). The cree tests in air were conducted in Mayes TC high sensitivity constant load creep testing machines with a microprocessor control and self-adaptive temperature control.

Table 1 – Chemical Composition of AISI 310S Stainless Steel

C	Mn	P	S	Si	Cr	Ni	Fe
0.08	1.25	0.045	0.03	0.96	24.8	18.5	Balance
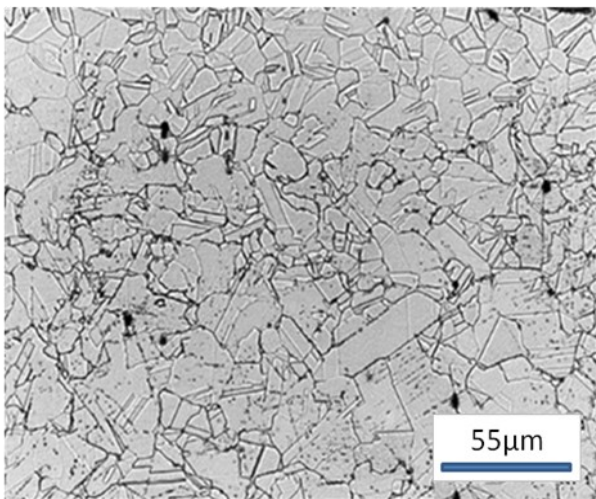
Figure 1 - Grain structure of AISI 310 stainless stee with an average grain size of 55 µ m (annealed)

Table 2 - Data used to draw deformation map of AISI 310 stainless steel

Property /constant	Numerical value	Property /constant	Numerical value
A	1010	b	2.58×10^{-10}m
B	14	d	5.5×10^{-5}m
C	50	Qv	280kJ/mol
n	6.5	Qg	167kJ/mol
Tm	1670K	D_{v0}	3.7×10^{-5}m^2/s
		D_{g0}	2×10^{-13}m^2/s

A detailed experimental procedure is available elsewhere [2]. The accuracy in the measurements are: load ±1N, temperature ±1K, creep strai ±0.002% and time ± 360s. The plot of applied stres versus the minimum cree rate was used to get the stress exponen (n) was evaluated. The value of stress exponent is 6.5 at all test temperatures (973K, 1023K and 1073K). From the observed value of stress exponent, it can be said that high temperature climb is operating mechanism. The effect of temperature on minimum creep rate was also considered for discussion regarding activation energ of the aforesaid creep mechanism. The activation energy (derived from the slope), Qc, is found to be 345kJ/mol which is larger than the activation energy for self-diffusio in pure FCC iron, i.e., 270-311kJ/mol. This indicates that the alloying elements are involved in the dislocation network recover coarsening process during creep [3, 6, 7]. In short, present test temperatures 973–1073K and stresses 40–150MPa fall in the power-law creep (dislocation creep) region in deformation map. The region is governed by diffusion-controlled climb-plus-glide processes such as (a) based on lattice diffusion-controlled climb (high-temperature creep), (b) based on core diffusion-controlled dislocation climb (low-temperature creep), and (c) transition from climb-plus-glide to glide alone (power law breakdown).
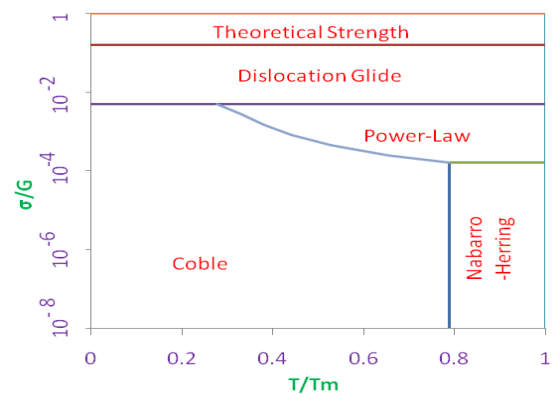
Figure 2 - Deformation map for AISI 310 stainless steel having an average grain size of 55 µ m.

Creep Fracture Map

"Table 3" lists the various properties and constants used in the generation of cree fracture map. "Figure 3" shows the cree fracture map for AISI 310 austenitic stainless stee sheets having an average grain size of 55µm in the form of logarithmic normalised stres (σ/G) versus the reciprocal of homologous temperature (Tm/T). The values of σ/G ranges between 10^{-4} and 10^{-1} whilst Tm/T ranges from 2.8 to 1.0 ($\approx$600-1670K). Even though the experiments were conducted at temperature above 0.5Tm (i.e., the experimental temperature range is from 0.58Tm to 0.64Tm), all the points fall in the low temperature regime of triple point cracking domain. This is due to the assumption that the various fracture mechanisms are operative independently. It is thus relatively simple process to use the theoretical relationships to construct creep fracture map for AISI 310 stainless stee sheets having an average grain size of 55µm and stress exponen of 6.5. The accuracy of the map, however, depends critically on the accuracy of both the theoretical processes and the material parameters used in its construction.

An important prerequisite of this approach is therefore is to check whether the predicted results are in reasonable agreement with the experimental observations. The fractured creep specimens were analyzed under a Jenavert optical microscope [2]. Theoretical findings are exactly matching the experimental data. As far as the experimental observation of cree fracture is concerned, it occurs in three steps:

(a)   nucleation of cracks,

(b)   stable growth of cracks and

(c)   unstable crack growth leading to final fracture.

Table 3 -Data used to Generate Creep Fracture Map of AISI 310 Stainless Steel Sheet

Property/ constant	Numerical value	Property/ constant	Numerical value
D_{v0}	$1.5 \times 10^{-5} \text{m}^2/\text{s}$	N	6.5
Q_v	260kJ/mol	A	10^{10}
δD_g	3.0×10^{-14} m^3/s	ε_n	0.1
D_{g0}	2.0×10^{-13} m^2/s	f_v	0.1
Q_g	195kJ/mol	γ	200J/m^2
R	8.31J/K/ mol^1	ξ	0.2
T_m	1670K	l	10^{-5}m
G	$8.1 \times 10^{10} \{1-[4.7 \times 10^{-4}(T-300)]\}$ Pa	A_0	0.24
b	2.58×10^{-10}m	l_0	5×10^{-6}m
d	5.5×10^{-5}m	P_o	1.5×10^{-6}m

It is generally accepted that inter-granular creep fracture occurs by the formation of three alternative types of crack or voi. They are inter-granular cavities, inter-granular wedge cracks and plastic growth of holes. An optical microscopic examination made in the present study though supported the occurrence of inter-granular creep fracture, branching internal crack and wedge type cracks, the latter type of cracks are mainly seen at all test temperatures. The wedge cracks starts at 45° to the loading direction and maintains approximately at 90° in the fully formed condition. An optical micrograph of the crept specimen after 42ks at 1023K and 94.6MPa is quite good for discussion ("Figure 4"). Wedge type cracks are visible and are observed approximately at 90° to the loading direction. The extensive grain-boundary sliding was responsible for the rapid increase in crack formation. The wedge type cracks were observed mainly at triple points. In general, the triple point cracks are nucleated at low

strains during cree at relatively high stress levels. Thus, in short, the prediction from creep fracture map and experimental results strongly support triple point crackin or wedge cracking as the operating mechanism of creep fracture in the present experimental conditions, i.e., at the operating temperature of 973-1073K and an applied stres range of 40-150MPa for AISI 310 stainless steel sheets a having grain size 55µm.
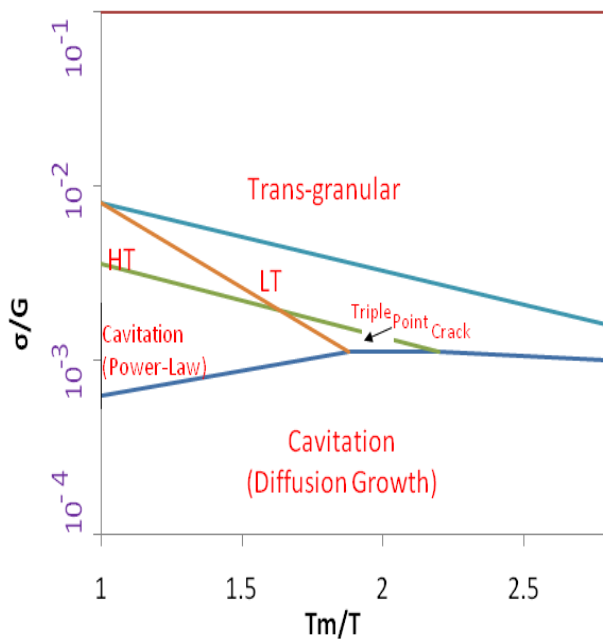
Figure 3- Fracture map for AISI 310 stainless steel sheet having a grain size of 55 µ m.

The microstructures of crept samples are in good correlation well with typical of literature data. For the alloy, mostly equi-axed and coarse grains extended to the whole cross section. The grains appear to be due to grain growth at high temperature. In "Figure 4", microstructure at near ruptured surface of crept sample of is clearly visible. Volume fraction of twins is normal and on the other hand extensive amount of carbides phase was present. Generally, at all test conditions, the alloy suffers from formation of cree cavities. The twins are clearly visible. Many representative micrographs seen elsewhere clearly explain formation of creep cavities, twins and oxide scales [2].
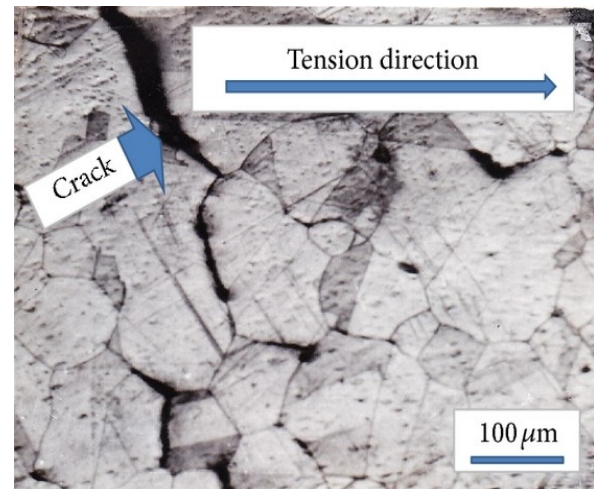
Figure 4 - Micrograph of crept sample at test temperature 1073K and applied stress 66.6MPa

These features are usually controlled by heat treatment. On the other hand, alloying chemistry influences the creep properties by solid solution or precipitation strengthening. Therefore, micro-structural control and alloying chemistry influences the creep properties by two different avenues. However, controlled alloying chemistry, e.g. in this present study; systematic heat treatment provides a path to study the minor effect of alloying chemistry on micro-structural features. The result of micro-structural characterization shows twins and grain size is found to be in a similar range for all the specimens investigated. Therefore, it is concluded that alloy chemistry and heat treatment does not have significant effect on micro-structural features. The variation in creep properties between the alloy studied and super-allo is solely on the strengthening mechanism and phases present [8]. Even though it had been reported that solid solution strengthenin by addition of Cr increases the creep life at high stresses, however it has no significant effect to the applications. This is due the creep strai exhibited by solid solution strengthening is only lesser than super-alloy. Aerospace and automotive applications not only concerns with creep life but creep strain too. Steady state creep

rate and the time necessary to reach 1% creep strain are slightly high or not significantly high. From the present study, it is concluded that solid solution strengthening does not have significant effect on creep strengt of the alloy and introducing many alloying elements is found to be detrimental for creep strength with respect to the applications [2].

IV. CONCLUSIONS

In summary, a systematic analysis of the results has led to the following conclusions. It is known from deformation mechanism map that AISI 310 stainless stee sheets follow a recover controlled cree (power-law creep) as the operating mechanism at an applied temperature range of 973-1073K and an applied stres range of 40-150MPa. Also, from the observed value of stress exponent (6.5, it can be said that high temperature clim is the operating mechanism. The experimental value of creep activation energ (Qc) is equal to 345kJ/mol which is larger than the activation energy for self-diffusio in pure FCC iron, i.e., 270-311kJ/mol. This indicates that the alloying elements are involved in the dislocation network recovery coarsening process during creep.

It is seen from the cree fracture maps that creep fracture occurred in the present case by triple point crackin (wedge cracking). Optical microscopic examination supported the presence of inter-granular cree fracture of wedge type cracks (triple point cracks) formed approximately perpendicular to the loading direction. Thus, the prediction from cree fracture map and experimental results support triple point crackin or wedge cracking as the operating mechanism of creep fracture in the present experimental conditions, i.e., at an applied temperature range of 973-1073K and an applied stres range of 40-150MPa.

REFERENCES:

[1] Rishi Raj, Flow and fracture at high temperature, (Metals Park:ASM International, 2018)

[2] A. Kanni Raj, On High-Temperature Materials: A Case on Creep and Oxidation of a Fully Austenitic Heat-Resistant Super-alloy Stainless Steel Sheet, *Journal of Materials*, Vol. 2013, Article ID 124649, 6 pages, doi:10.1155/2013/124649

[3] M. E. Kassner, and M. T. Perez Prado, Five-power-law creep in single phase metals and alloys, *Progress in Materials Science*, 45(1), 2000, 1–102.

[4] N.Bano, A.K. Koul, and M.Nganbe, A deformation mechanism map for the 1.23Cr-1.2Mo-0.26V rotor steel and its verification using neural networks, *Metallurgical and Materials Transactions A*, 45(4), 2014, 1928–1936

[5] S.N. Monteiro, L.P.M. Brandão, A.D.S. Paula, C.N. Elias, A.C. Pereira, F.S.D. Assis, L.H.D.Almeida, and L.S. Araújo, Creep fracture mechanisms and maps in AISI type 316 austenitic stainless steels from distinct origins, *Materials Research*. 20(2), 2017, 892-898

[6] K. Maruyama, H. Ghassemi Armaki, and K. Yoshimi, Multi-region analysis of creep rupture data of 316 stainless steel, *International Journal of Pressure Vessels and Piping*, 84(3), 2007, 171–176

[7] R. Voicu, J. Lacaze, E. Andrieu, D. Poquillon, and J. Furtado, Creep and tensile behavior of austenitic Fe-Cr-Ni stainless steels, *Materials Science and Engineering*, 510A-511A, 2009, 185–

189.

[8]   H. De Cicco, M. I. Luppo, H. Raffaeli, J. Di Gaetano, L. M. Gribaudo, and J. O.García, Creep behavior of an A286 type stainless steel, *Materials Characterization*, 55(2), 2005, 97–105

* * * * *